Appl Nanosci (2015) 5:425–433
DOI 10.1007/s13204-014-0334-1

ORIGINAL ARTICLE

2-Aminoethanol-mediated wet chemical synthesis of ZnO nanostructures

Tehmina Naz · Adeel Afzal · Humaira M. Siddiqi · Javeed Akhtar · Amir Habib · Mateusz Banski · Artur Podhorodecki

Received: 13 April 2014 / Accepted: 27 June 2014 / Published online: 19 July 2014

Abstract The synthesis of ZnO nanostructures via co-precipitation of $Zn(NO_3)_2{\cdot}2H_2O$ in 2-aminoethanol under different reaction conditions is presented. The effect of temperature and time on crystal structure, size, morphology, and optical properties of ZnO nanopowders is studied. XRD analyses demonstrate that single crystalline wurtzite ZnO nanostructures are instantaneously formed at higher temperature, or at low temperature with growth times equal to 2 h. However, the mean crystallite size increases as a function of reaction temperature and growth time. XRD and SEM results reveal that ZnO nuclei grow along favored crystallographic planes [wurtzite (101)] in 2-aminoethanol to form single crystalline nanorods. The optical band-gap energies of ZnO crystallites measured from their UV absorption spectra increase from 3.31 to 3.52 eV with decreasing particle size. ZnO nanopowders also exhibit good photoluminescent characteristics with strong UV and weak visible (violet, blue) light emissions corresponding to surface defects and oxygen vacancies in ZnO products.

Keywords 2-Aminoethanol · Band gap · Crystallite size · Photoluminescence · ZnO nanostructures

T. Naz · A. Afzal (✉) · H. M. Siddiqi (✉)
Department of Chemistry, Quaid-i-Azam University, Islamabad 45320, Pakistan
e-mail: aa@aafzal.com

H. M. Siddiqi
e-mail: humairas@qau.edu.pk

A. Afzal
Affiliated Colleges at Hafr Al-Batin, King Fahd University of Petroleum and Minerals, P.O. Box 1803, Hafr Al-Batin 31991, Saudi Arabia

J. Akhtar
Department of Physics, COMSATS Institute of Information Technology, Islamabad Campus, Chak Shahzad, Islamabad 44000, Pakistan

A. Habib
School of Chemical and Materials Engineering, National University of Science and Technology, H-12, Islamabad 44000, Pakistan

M. Banski · A. Podhorodecki
Institute of Physics, Wroclaw University of Technology, Wybrzeze Wyspianskiego 27, 50-370 Wroclaw, Poland

Introduction

In the past few years, ZnO-based nanostructured materials have emerged as the first-choice materials not only for semiconductor devices such as sensors (Chougule et al. 2012; Afzal et al. 2012) and solar cells (Kim et al. 2013; Patra et al. 2014), but also in other fields as UV emitters (Zhang et al. 2013), optical waveguides (Jiang et al. 2012), and biomedical (Yang et al. 2012) and optoelectronic devices (Zhang et al. 2012). The nontoxic nature, low cost, stability, easy processability, and nanostructuring are the chief distinctions of ZnO (Schmidt-Mende and MacManus-Driscoll 2007).

A wide range of synthetic methods are currently available for developing different morphologies of ZnO nanostructures, which result in a variety of material applications such as those mentioned above (Djurišić et al. 2012). These include hydrothermal, sol–gel, sonochemical, organometallic, pyrolysis, laser ablation, and vapor phase epitaxial growth (Schmidt-Mende and MacManus-Driscoll 2007; Djurišić et al. 2012; Wang 2004; Ismail et al. 2011; Samanta and Bandyopadhyay 2012; Zhan et al. 2012) synthetic methods. It is well known that physical properties of

thus obtained ZnO nanostructures radically depend on the choice of the synthetic method.

In the recent past, researchers have also used different structure-directing agents to prepare ZnO nanomaterials and to optimize their structure, morphology, and properties (Shouli et al. 2010; Aimable et al. 2010; Veriansyah et al. 2010; Rai and Yu 2012; Foe et al. 2013). These structure-directing agents include simple organic molecules such as methanol, ethanol, amines, and urea, specialized surfactants such as cetyltrimethylammonium bromide (CTAB), trisodiumcitrate, and sodium dodecyl sulfate (SDS), and polymers such as polyethylene glycol (PEG), polyvinylpyrrolidone (PVP), and poly(acrylic acid). These reagents principally control the rate of reaction, growth of ZnO crystals, morphology (size, shape, and distribution), and physical properties of the final ZnO products.

In this bargain, the researchers successfully prepared different forms of ZnO nanostructures by precipitating aqueous zinc salt solutions with NaOH in the presence of small amounts of aminoethanol (Costa and Baptista 1993; Wang et al. 2011). Wang et al. (2011) specially studied the effect of aminoethanol and NaOH concentration on the morphology of ZnO nanostructures synthesized via one-pot hydrothermal synthesis. They concluded that varying ethanolamine concentration had a pronounced effect on the morphology and structure of ZnO nanopowders due to competitive adsorption of aminoethanol and $[Zn(OH)_4]^{2-}$ on ZnO nuclei.

Herein, we further exploit 2-aminoethanol as the structure-directing agent in the wet chemical synthesis of ZnO nanopowders. While the concentration of aminoethanol is fixed during these experiments, reaction conditions such as temperature and time are varied to study their effects on the crystalline nature, crystallite size, morphology, and optical properties including UV emission, band gap, and photoluminescent characteristics of the so formed ZnO nanopowders. Furthermore, in our experiments, 2-aminoethanol is used as the solvent for $Zn(NO_3)_2$, while it also acts as a surfactant and selectively adsorbs on growing ZnO nuclei to facilitate preferred growth on certain crystallographic planes, thus resulting in the formation of hexagonal ZnO nanorods. The temperature and time are found to increase the crystallite size. It is found that ZnO nanopowders show weak violet and blue emissions along with stronger UV emission.

Experimental

Chemicals and reagents

All chemicals were used as received without further purification. Zinc nitrate hexahydrate ($Zn(NO_3)_2{\cdot}6H_2O$; crystallized, ≥99.0 %) was purchased from Sigma-Aldrich. 2-Aminoethanol (ACS reagent, ≥99.0 %) was obtained from Fluka. Liquid ammonia (33 %) was received from Lab-Scan. Ethanol (anhydrous) was obtained from Sigma-Aldrich.

Synthesis of ZnO nanostructures

ZnO nanopowders of variable sizes and morphology were synthesized by co-precipitation of $Zn(NO_3)_2{\cdot}6H_2O$ in 2-aminoethanol. For this purpose, 2-aminoethanol (20 mL) was placed in a 250-mL round-bottom flask. $Zn(NO_3)_2{\cdot}6H_2O$ (14 mmol; 4.15 g) was then added into the flask and dissolved through ultrasound sonication for several minutes. After the clear solution of $Zn(NO_3)_2{\cdot}6H_2O$ in 2-aminoethanol was obtained, liquid NH_3 (10 mL) was added slowly to the mixture. The mixture was subsequently diluted with a small amount of deionized water to attain a pH of 11.2. From this point onward, the temperature and time of the reaction were controlled to study the effect of increasing temperature and time on crystallinity, geometry, surface morphology, and optical properties of ZnO nanostructures. The temperature of the reaction was varied between 60 and 94 °C, whereas growth time was varied in the range of 15–120 min.

Table 1 provides details of the reaction times and temperatures adapted in different procedures to prepare ZnO nanopowders. White precipitates of ZnO nanopowders were obtained after the completion of these reactions. The solvent (2-aminoethanol) and excess water were decanted off after centrifuge, and the products (white powders) were dried in an oven at 100 °C. The colloidal suspensions of

Table 1 The optimization of reaction conditions (time and temperature) to obtain different ZnO nanostructures

Experiment	Growth time (min)	Reaction temperature (°C)	Crystallite size (nm)	Sample ID
Series A	60	60	12.50 ± 0.92	ZnO-A60
		70	33.82 ± 1.20	ZnO-A70
		75	40.28 ± 1.20	ZnO-A75
		80	43.15 ± 1.29	ZnO-A80
		94	65.40 ± 1.97	ZnO-A94
Series B	15	60	9.80 ± 0.50	ZnO-B15
	30		10.66 ± 0.65	ZnO-B30
	60		12.50 ± 0.92	ZnO-B60
	120		15.26 ± 1.05	ZnO-B120
Series C	15	94	35.62 ± 1.23	ZnO-C15
	30		40.28 ± 1.54	ZnO-C30
	60		65.40 ± 1.97	ZnO-C60
	120		69.50 ± 1.54	ZnO-C120

different ZnO nanopowders were prepared in anhydrous ethanol by ultrasound sonication for 15 min for the purpose of analytical characterization.

Analytical methods

X-ray diffraction (XRD) patterns of as-synthesized ZnO nanostructures were obtained by Siemens D500 XRD instrument equipped with Cu Kα irradiation source (wavelength: 1.5406 Å), at 40 kV and 30 mA. XRD patterns were obtained at a scanning rate of 10° min^{-1} from 10° to 80° of 2θ.

The surface morphology of synthesized ZnO nanostructures was studied on Jeol JFM 5910 SEM instrument equipped with tungsten filament electron emitter at an accelerating voltage of 5–10 kV.

The selected ZnO nanoparticle suspensions in ethanol were also characterized by UV–vis spectroscopy at 25 °C. A Schimadzu UV–vis spectrophotometer, model Pharma Spec UV-1700, and quartz cuvette were used for this purpose. The photoluminescence (PL) spectra were also measured at room temperature at an excited wavelength of 296 nm.

Results and discussion

The structural characterization of ZnO nanopowders

The structural characterization of ZnO nanopowders to determine their crystallinity, crystal phase characteristics, and purity was performed with the help of XRD. Figure 1 shows the XRD patterns of different ZnO samples belonging to series A. These nanopowders were prepared in 2-aminoethanol at different temperatures (60–94 °C) with a constant growth time of 60 min. The reference XRD patterns and relative peak intensity of phase-pure hexagonal wurtzite and cubic ZnO are also provided in Fig. 1 for comparison.

It is evident that ZnO nanopowders obtained at lower temperatures, e.g., ZnO-A60, ZnO-A70, and ZnO-A75 prepared at 60, 70, and 75 °C, respectively, do not exhibit phase-pure crystalline structure. Instead, these ZnO nanopowders show the characteristics of both hexagonal wurtzite and cubic phases along with some impurities such as $Zn(OH)_2$ (Yang et al. 2006; Rai and Yu 2012). It is due to the fact that as-synthesized ZnO nanopowders at low temperature are not treated thermally at higher

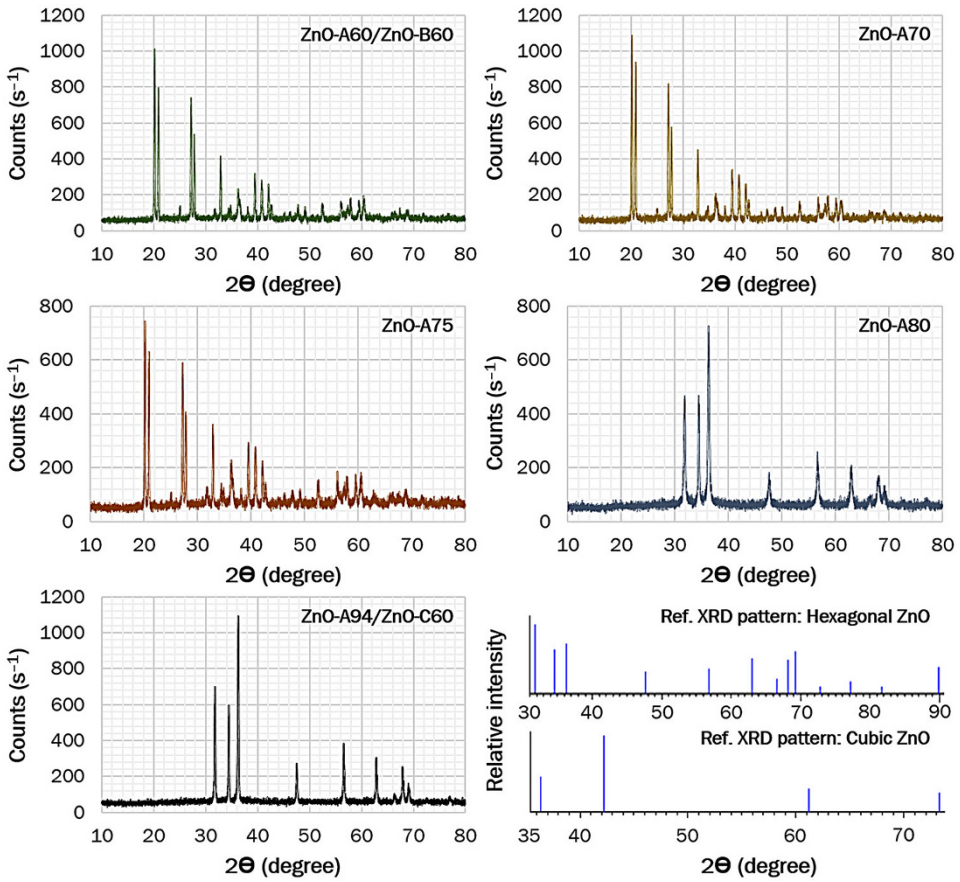

Fig. 1 XRD patterns of ZnO nanopowders (series A) prepared in 2-aminoethanol at different temperatures. The reference XRD patterns of crystalline hexagonal wurtzite and cubic ZnO are also given for comparison

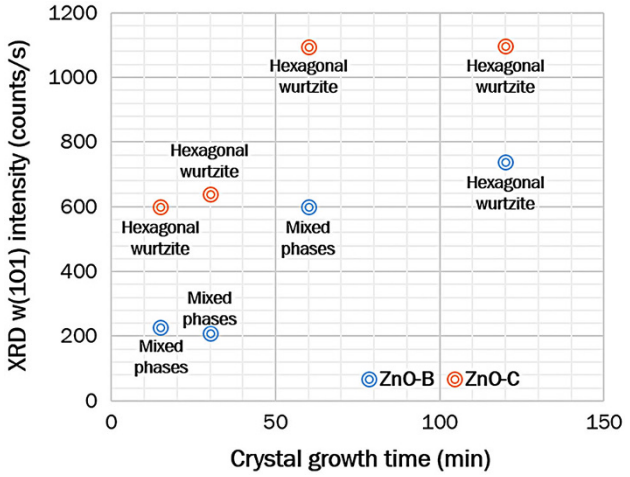

Fig. 2 The primary wurtzite diffraction peak w(101) intensity plotted as a function of reaction time. The crystalline nature of ZnO nanostructures is also indicated

temperature, thus they retain some functional hydroxyl groups on the surface.

However, ZnO nanopowders synthesized at higher temperatures, e.g., at 80 °C (ZnO-A80) and at 94 °C (ZnO-A94) show crystalline structure and their XRD reflections can be indexed as hexagonal wurtzite ZnO phase (Guo et al. 2002; Geng et al. 2004), i.e., the results are in agreement with the standard hexagonal wurtzite ZnO crystal structures with space group P63mc. The respective XRD patterns indicate that these ZnO nanopowders obtained at higher temperature were phase-pure single crystalline powders with no observable peaks relevant to impurities such as $Zn(OH)_2$. The sharp XRD peaks in ZnO-A94 also suggest that ZnO-A94 nanopowders are well crystallized as compared to ZnO-A80.

The XRD patterns of ZnO nanopowders corresponding to series B and C were also observed. The diffraction peaks around 31.8°, 34.5°, and 36.3° 2θ positions, which are indexed as w(100), w(002), and w(101) planes of wurtzite crystal, respectively, were observed in each sample indicating the existence of a wurtzite crystal structure. However, the samples of series B (prepared at 60 °C) also exhibit XRD peaks corresponding to the cubic phase and $Zn(OH)_2$ impurities, except ZnO-B120 that has wurtzite crystalline structure. On the other hand, all samples of ZnO nanopowders (belonging to series C) have single crystalline wurtzite structure.

Figure 2 shows the intensity of w(101) XRD peak, i.e., major wurtzite diffraction in series B and C samples of ZnO nanopowders plotted as a function of reaction/growth time. The crystalline nature of all samples is also indicated in Fig. 2. It is found that higher reaction temperature or prolonged reaction time is required to prepare hexagonal wurtzite ZnO nanostructures in 2-aminoethanol as the reaction medium. Therefore, we conclude that slightly higher temperature is needed for the growth of wurtzite crystal structures, although the formation of ZnO nanophases is thermodynamically favored under ambient conditions. Likewise, for reactions carried out at lower or room temperatures, additional time is needed for crystal growth.

XRD analyses also offer further structural information on the crystallite size of ZnO nanostructures. The mean crystallite size of various ZnO nanopowders can be calculated by using the Scherrer's formula that is given in the following equation: ($D = 0.9\lambda/B\cos\theta$), where D is the mean crystallite size of the ZnO nanopowder, λ is the wavelength of Cu Kα radiation, i.e., $\lambda = 1.5406$ Å, B is the full-width-at-half-maximum (FWHM) intensity of the diffraction peak in radian, and θ is the Bragg's diffraction angle (Mahmood et al. 2013). Consequently, the mean crystallite size of different samples of ZnO nanopowders was measured and reported in Table 1. It is found that the mean crystallite sizes of different ZnO nanopowders synthesized under different reaction conditions of time and temperature lie in the range 9.8–69.5 nm.

Effect of temperature on mean crystallite size of ZnO nanopowders

The mean (or average) crystallite size of ZnO nanopowders (series A) prepared in 2-aminoethanol at different temperatures (60–94 °C) and constant reaction time of 60 min are determined from the respective XRD patterns. These crystallite sizes are plotted as a function of reaction temperature in Fig. 3. It is obvious that a straight trendline is obtained that shows a regular increase in the mean crystallite size as a function of reaction temperature.

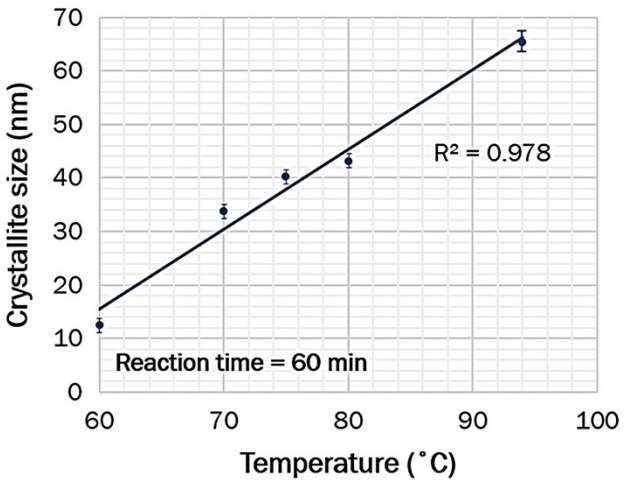

Fig. 3 The mean crystallite size of ZnO nanopowders synthesized in 2-aminoethanol at different reaction temperature (60 °C) and constant growth time of 60 min

Amin et al. (2011) reported that the surface area of hydrothermally grown ZnO nanostructures increases as a function of temperature within the temperature range of 50–90 °C, which is an indication of decreasing particle size with increasing temperature. However, we observed different results during the wet chemical synthesis of ZnO nanopowders involving 2-aminoethanol as a solvent as well as a surfactant, which indicates a regular growth in the mean crystallite size of the so formed ZnO nanopowders as a function of increasing temperature in the range of 60–94 °C. This may be attributed to an increased growth rate of wurtzite ZnO crystals at higher temperature that leads to relatively larger mean crystallite size.

Effect of growth time on mean crystallite size of ZnO nanopowders

The mean crystallite size of ZnO nanopowders belonging to the experimental series B and C were also measured from the respective diffraction patterns to study the effect of growth (reaction) time on crystallite size. These ZnO nanopowders were prepared in 2-aminoethanol at a constant temperature of 60 (series B) or 94 °C (series C), while growth time was varied from 15 to 120 min. Figure 4 shows the crystallite size of various ZnO samples as a function of growth time. It is obvious from the linear trendline that the mean crystallite size of ZnO nanopowders consistently increases with the increasing growth time.

These results are well in agreement with previous reports on hydrothermal and microwave-assisted synthesis of ZnO nanostructures (Amin et al. 2011; Barreto et al. 2013). For ZnO nanopowders prepared in 2-aminoethanol, it is found that with an increase in reaction time while maintaining constant temperature, concentration and pH, ZnO nanocrystallites continue to grow and form bigger ZnO nanocrystallites. Furthermore, the nucleation and growth of ZnO nanocrystallites is faster at higher temperature (94 °C) leading to much bulkier single crystalline ZnO nanostructures, whereas the growth of ZnO nanocrystallites is slow at low temperature (60 °C) giving rise to smaller and mixed phase ZnO powders (Rai et al. 2011).

The surface morphology of ZnO nanopowders

The suspensions of ZnO nanopowders prepared in ethanol by sonication were coated on quartz slides to monitor the surface morphology, i.e., size, shape, and distribution, of ZnO nanopowders. Figure 5 shows the SEM micrograph of ZnO-A60 or ZnO-B60 sample corresponding to ZnO nanopowders prepared at 60 °C and with 60 min of growth time. The image demonstrates that ZnO nanopowders are composed of small ZnO nanoparticles of sizes equal to ~20 nm. These ZnO nanoparticles are non-agglomerated and uniformly distributed on the surface with a narrow particle size range. The size of ZnO nanoparticles obtained from the SEM image is slightly greater than the mean crystallite size (12.5 nm) determined from the respective XRD patterns.

Figure 6 shows the SEM image of ZnO-A94 or ZnO-C60 sample corresponding to ZnO nanopowders prepared at 94 °C and with 60 min of growth time. The micrograph shows completely different surface morphology as compared to ZnO nanopowders prepared at lower temperature. In this case, ZnO-A94 nanopowders are composed of hexagonal nanorods, with edge-to-edge distance of ~200 nm. In addition, these nanorods are aligned on quartz surface in the shape of a flower with six nanorods surrounding a single vertically aligned central nanorod,

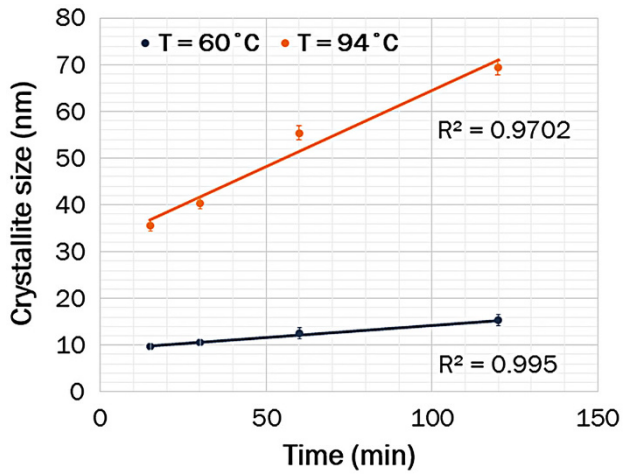

Fig. 4 The mean crystallite size of ZnO nanopowders synthesized in 2-aminoethanol at constant reaction temperatures of 60 and 94 °C and different growth times varying between 15 and 120 min

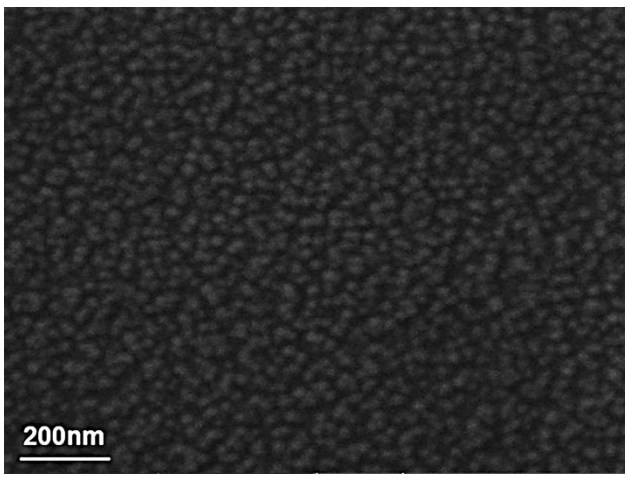

Fig. 5 The surface morphology of ZnO nanopowders synthesized in 2-aminoethanol at 60 °C with 60 min of growth time (sample ID: ZnO-A60/ZnO-B60)

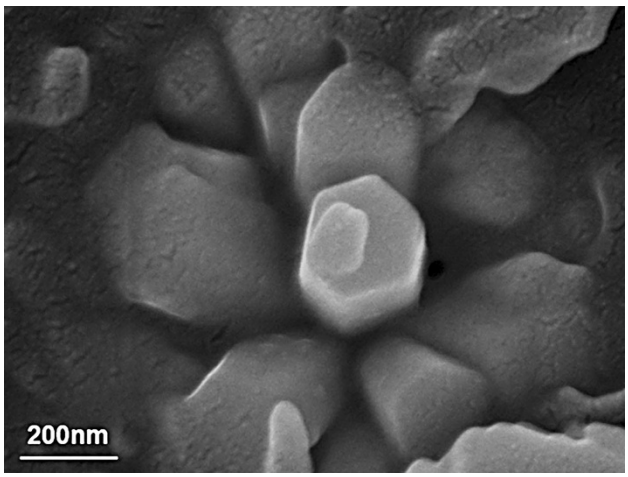

Fig. 6 The surface morphology of ZnO nanopowders synthesized in 2-aminoethanol at 94 °C with 60 min of growth time (sample ID: ZnO-A94/ZnO-C60)

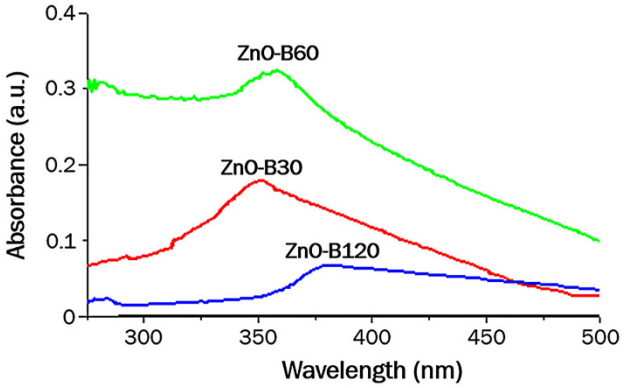

Fig. 7 UV–vis spectra of ZnO nanopowders (series B) prepared in 2-aminoethanol at constant temperature (60 °C)

thus forming a narcis-like architecture (Kajbafvala et al. 2010).

The difference in surface morphology of ZnO nanopowders synthesized under different conditions of temperature is obvious, and it may be attributed to faster and selective crystal growth on ZnO nuclei at higher temperature. In the respective diffraction patterns of ZnO nanopowders such as that of ZnO-A94 (in Fig. 1), it is clear that the diffraction peak corresponding to the w(101) plane of wurtzite crystal structure is the most intense peak, whereas the reference XRD pattern of hexagonal wurtzite structure shows the diffraction peak corresponding to w(100) plane as the most intense diffraction signal.

This fact supports the preferential growth mechanism of ZnO nanocrystallites along a particular lattice plane, i.e., w(101) that leads to the formation of ZnO nanorods (Nirmala et al. 2010; Rai et al. 2011). The preferential growth of ZnO nanocrystallites in a particular crystallographic plane may be attributed to the presence of 2-aminoethanol, which hereby acts as the structure-directing agent. 2-aminoethanol, the solvent used in the synthesis of ZnO nanopowders, also acts as a surfactant or capping agent, which may alter the relative growth of ZnO crystallites by adsorbing on specific crystallographic planes of the growing ZnO nuclei, thus inhibiting growth along these planes (Harunar Rashid et al. 2009). This may ultimately result in the formation of single crystalline wurtzite nanorods.

UV–vis spectroscopy and optical band-gap calculations

In recent years, wide band-gap semiconductors such as ZnO have attracted the scientific community due to increasing commercial demands of short wavelength light-emitting devices. ZnO is a wide band-gap (3.3 eV) semiconductor with a high excitation binding energy (60 meV) (Caglar et al. 2010). In general, bulk ZnO can absorb UV radiations with the wavelength $\leq$385 nm (Nirmala et al. 2010). The UV–vis absorption spectra of ZnO nanopowders prepared in 2-aminoethanol under controlled reaction conditions are shown in Fig. 7. The UV–vis absorption spectra were obtained from ZnO nanopowder suspensions in anhydrous ethanol. For this purpose, we have chosen ZnO nanopowders having smaller mean crystallite size, i.e., those belonging to the series B, as shown in Table 1. These ZnO nanopowders were prepared at a constant temperature of 60 °C, but growth time was varied between 15 and 120 min.

The mean crystallite size of these nanopowders varies in the range of 9.8–15.3 nm. The UV–vis absorption spectra of ZnO nanopowders exhibit well-defined excitation bands in the range of 350–375 nm showing a significant shift as compared to the bulk ZnO (Nirmala et al. 2010). The stronger UV emission of ZnO nanopowders in this range corresponds to the excitation of electrons from the valence band to the conduction band. At room temperature, these excellent UV emission properties of ZnO nanopowders may be attributed to the crystalline nature and small size of the synthesized ZnO nanopowders (Kajbafvala et al. 2010).

Furthermore, these UV absorptions can be used to calculate the band gap ZnO nanopowders using the following equation: ($E = hc/\lambda$). While bulk ZnO has a band-gap energy of 3.3 eV at room temperature, the band gap of nanoscale ZnO generally increases with decreasing particle size due to quantum confinement (Ceylan et al. 2013). Therefore, we have chosen (series B) ZnO nanopowders for their smaller mean crystallite size. The band-gap energies calculated from their UV absorptions are found to be 3.52, 3.46, and 3.31 eV for ZnO-B30, ZnO-B60, and ZnO-B120 samples, respectively. Thus, we found that ZnO

nanopowders with the mean crystallite size larger than 16 nm would have same band-gap energies as bulk ZnO.

It was also observed that a decrease in ZnO crystallite size from 15.3 to 10.7 nm enhanced the band-gap energy from 3.31 to 3.52 eV. This is expected since with the decrease in crystallite size, the energy gap between the valence band and the conduction band increases and more energy is required for electronic transitions. Thus, smaller size particles absorb a higher amount of energy (corresponding to lower wavelengths) and show maximum UV absorption at comparatively shorter wavelength as compared to larger size particles and bulk ZnO.

Photoluminescence characteristics

The photoluminescent behavior of ZnO nanopowders draws particular concern from the academic and applied research viewpoints. The luminescent ZnO nanostructures are promising for their applications in UV lasing devices, sensors, and bio labeling due to their cost-effectiveness and nontoxic characteristics (Xiong et al. 2011). We studied the photoluminescent properties of the selected samples of ZnO nanopowders (series A) due to a variety of crystallite sizes, difference in crystallinity, and phase purity. Figure 8 shows the typical photoluminescence (PL) spectrum of ZnO nanopowders prepared at 60 (ZnO-A60/ZnO-B60) and 94 °C (ZnO-A94/ZnO-C60). The mean crystallite size of the ZnO nanopowders obtained at 60 and 94 °C is 12.5 and 65.4 nm, respectively.

Evidently, ZnO-A60 and ZnO-A94 nanopowders demonstrate a sharp near-band-edge UV emission at 365 and 376 nm. The sharp near-band-edge emissions may be attributed to the well-known recombination of excitonic transitions (Bekeny et al. 2006; Buyanova et al. 2007). In addition, a few weak emission bands can be observed in the range of 420–430 nm corresponding to violet emission in both of these spectra. The source of violet emission band has been identified by Zeng et al. (2006) as the electronic transition from the high-concentration Zn interstitial defect levels to the valence band.

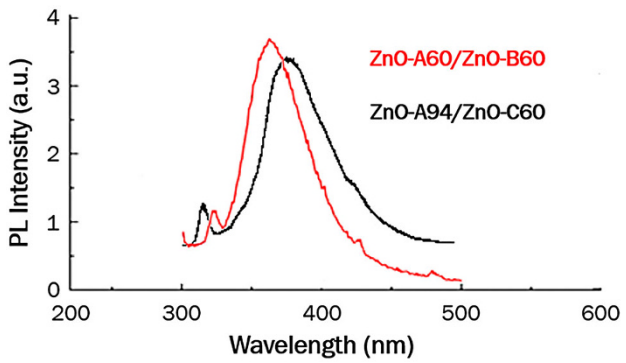

Fig. 8 Typical photoluminescence spectra of ZnO nanoparticles and ZnO nanorods prepared in 2-aminoethanol at 60 and 94 °C, respectively

Furthermore, ZnO-A60 shows another weak emission band at 476 nm corresponding to blue emission, which is not observed in ZnO-A94 nanopowders. Blue emission band is also attributed to the crystal defects in ZnO nanopowders and electronic transitions from the lower levels of oxygen vacancies to the valence band (Xue et al. 2002; Zeng et al. 2010). Thus, it is concluded that ZnO nanopowders produced in 2-aminoethanol inherently possess zinc interstitials and oxygen vacancies, which give rise to such photoluminescent characteristics. The smaller ZnO crystallites produce relatively stronger and multiple emissions (violet and blue) in the visible region as compared to bigger ZnO crystallites.

Conclusions

The structural characterization, optical band gap, and photoluminescent characteristics of ZnO nanopowders prepared in 2-aminoethanol under different reaction conditions are presented in this article. The effects of reaction temperature, growth time, and 2-aminoethanol (solvent and surfactant) on crystallinity, mean crystallite size, morphology, and properties of synthesized ZnO nanopowders are investigated. We conclude that crystallite size is positively affected by increasing temperature due to increased growth rate as well as by increasing growth time, which end up in the formation of bulkier, single crystalline wurtzite ZnO nanostructures. When provided higher temperature or sufficient growth time, 2-aminoethanol acts as a structure-directing agent leading to preferred growth on the w(101) plane of wurtzite crystal and to the formation of nanorods. These ZnO nanorods align on quartz surfaces in the form of a narcis giving rise to a flower-like structure. The optical band gap of ZnO nanopowders is enhanced to 3.52 from 3.3 eV of bulk ZnO. Furthermore, photoluminescent studies demonstrate that ZnO nanopowders emit both UV and visible (violet and blue) radiation owing to some inherent oxygen vacancies and crystal defects in these ZnO nanostructures.

Acknowledgments The authors gratefully acknowledge the Higher Education Commission (HEC, Pakistan) for financial support under the National Research Program for Universities (NRPU) grant # 1308.

References

Afzal A, Cioffi N, Sabbatini L, Torsi L (2012) NOx sensors based on semiconducting metal oxide nanostructures: progress and perspectives. Sens Actuators B Chem 171–172:25–42. doi:10.1016/j.snb.2012.05.026

Aimable A, Buscaglia MT, Buscaglia V, Bowen P (2010) Polymer-assisted precipitation of ZnO nanoparticles with narrow particle size distribution. J Eur Ceram Soc 30:591–598. doi:10.1016/j.jeurceramsoc.2009.06.010

Amin G, Asif MH, Zainelabdin A et al (2011) Influence of pH, precursor concentration, growth time, and temperature on the morphology of ZnO nanostructures grown by the hydrothermal method. J Nanomater. doi:10.1155/2011/269692

Barreto GP, Morales G et al (2013) Microwave assisted synthesis of ZnO nanoparticles: effect of precursor reagents, temperature, irradiation time, and additives on nano-ZnO morphology development. J Mater doi:10.1155/2013/478681

Bekeny C, Voss T, Gafsi H et al (2006) Origin of the near-band-edge photoluminescence emission in aqueous chemically grown ZnO nanorods. J Appl Phys 100:104317. doi:10.1063/1.2390548

Buyanova IA, Bergman JP, Pozina G et al (2007) Mechanism for radiative recombination in ZnCdO alloys. Appl Phys Lett 90:261907. doi:10.1063/1.2751589

Caglar M, Caglar Y, Aksoy S, Ilican S (2010) Temperature dependence of the optical band gap and electrical conductivity of sol–gel derived undoped and Li-doped ZnO films. Appl Surf Sci 256:4966–4971. doi:10.1016/j.apsusc.2010.03.010

Ceylan H, Ozgit-Akgun C, Erkal TS et al (2013) Size-controlled conformal nanofabrication of biotemplated three-dimensional TiO_2 and ZnO nanonetworks. Sci Rep. doi:10.1038/srep02306

Chougule MA, Sen S, Patil VB (2012) Fabrication of nanostructured ZnO thin film sensor for NO_2 monitoring. Ceram Int 38:2685–2692. doi:10.1016/j.ceramint.2011.11.036

Costa MEV, Baptista JL (1993) Characteristics of zinc oxide powders precipitated in the presence of alcohols and amines. J Eur Ceram Soc 11:275–281. doi:10.1016/0955-2219(93)90026-N

Djurišić AB, Chen X, Leung YH, Ng AMC (2012) ZnO nanostructures: growth, properties and applications. J Mater Chem 22:6526–6535. doi:10.1039/C2JM15548F

Foe K, Namkoong G, Abdel-Fattah TM et al (2013) Controlled synthesis of ZnO spheres using structure directing agents. Thin Solid Films 534:76–82. doi:10.1016/j.tsf.2013.01.105

Geng C, Jiang Y, Yao Y et al (2004) Well-aligned ZnO nanowire arrays fabricated on silicon substrates. Adv Funct Mater 14:589–594. doi:10.1002/adfm.200305074

Guo L, Ji YL, Xu H et al (2002) Regularly shaped, single-crystalline ZnO nanorods with wurtzite structure. J Am Chem Soc 124:14864–14865. doi:10.1021/ja027947g

Harunar Rashid M, Raula M, Bhattacharjee RR, Mandal TK (2009) Low-temperature polymer-assisted synthesis of shape-tunable zinc oxide nanostructures dispersible in both aqueous and non-aqueous media. J Colloid Interface Sci 339:249–258. doi:10.1016/j.jcis.2009.07.011

Ismail RA, Ali AK, Ismail MM, Hassoon KI (2011) Preparation and characterization of colloidal ZnO nanoparticles using nanosecond laser ablation in water. Appl Nanosci 1:45–49. doi:10.1007/s13204-011-0006-3

Jiang DY, Zhao JX, Zhao M et al (2012) Optical waveguide based on ZnO nanowires prepared by a thermal evaporation process. J Alloys Compd 532:31–33. doi:10.1016/j.jallcom.2012.03.114

Kajbafvala A, Zanganeh S, Kajbafvala E et al (2010) Microwave-assisted synthesis of narcis-like zinc oxide nanostructures. J Alloys Compd 497:325–329. doi:10.1016/j.jallcom.2010.03.057

Kim H, Jeong H, An TK et al (2013) Hybrid-type quantum-dot cosensitized ZnO nanowire solar cell with enhanced visible-light harvesting. ACS Appl Mater Interfaces 5:268–275. doi:10.1021/am301960h

Mahmood Q, Afzal A, Siddiqi HM, Habib A (2013) Sol–gel synthesis of tetragonal ZrO_2 nanoparticles stabilized by crystallite size and oxygen vacancies. J Sol Gel Sci Technol 67:670–674. doi:10.1007/s10971-013-3112-8

Nirmala M, Nair MG, Rekha K et al (2010) Photocatalytic activity of ZnO nanopowders synthesized by DC thermal plasma. Afr J Basic Appl Sci 2:161–166

Patra AK, Dutta A, Bhaumik A (2014) Self-assembled ultra small ZnO nanocrystals for dye-sensitized solar cell application. J Solid State Chem doi:10.1016/j.jssc.2014.03.036

Rai P, Yu Y-T (2012) Citrate-assisted hydrothermal synthesis of single crystalline ZnO nanoparticles for gas sensor application. Sens Actuators B Chem 173:58–65. doi:10.1016/j.snb.2012.05.068

Rai P, Jo J-N, Wu X-F et al (2011) Synthesis of well dispersed, regular shape ZnO nanorods: effect of pH, time and temperature. J Nanosci Nanotechnol 11:647–651. doi:10.1166/jnn.2011.3178

Samanta PK, Bandyopadhyay AK (2012) Chemical growth of hexagonal zinc oxide nanorods and their optical properties. Appl Nanosci 2:111–117. doi:10.1007/s13204-011-0038-8

Schmidt-Mende L, MacManus-Driscoll JL (2007) ZnO: nanostructures, defects, and devices. Mater Today 10:40–48. doi:10.1016/S1369-7021(07)70078-0

Shouli B, Liangyuan C, Dianqing L et al (2010) Different morphologies of ZnO nanorods and their sensing property. Sens Actuators B Chem 146:129–137. doi:10.1016/j.snb.2010.02.011

Veriansyah B, Kim J-D, Min BK et al (2010) Continuous synthesis of surface-modified zinc oxide nanoparticles in supercritical methanol. J Supercrit Fluids 52:76–83. doi:10.1016/j.supflu.2009.11.010

Wang ZL (2004) Nanostructures of zinc oxide. Mater Today 7:26–33. doi:10.1016/S1369-7021(04)00286-X

Wang X, Zhang Q, Wan Q et al (2011) Controllable ZnO architectures by ethanolamine-assisted hydrothermal reaction for enhanced photocatalytic activity. J Phys Chem C 115:2769–2775. doi:10.1021/jp1096822

Xiong H-M, Ma R-Z, Wang S-F, Xia Y-Y (2011) Photoluminescent ZnO nanoparticles synthesized at the interface between air and triethylene glycol. J Mater Chem 21:3178. doi:10.1039/c0jm02577a

Xue ZY, Zhang DH, Wang QP, Wang JH (2002) The blue photoluminescence emitted from ZnO films deposited on glass substrate by r.f. magnetron sputtering. Appl Surf Sci 195:126–129

Yang M, Pang G, Jiang L, Feng S (2006) Hydrothermal synthesis of one-dimensional zinc oxides with different precursors. Nanotechnology 17:206–212. doi:10.1088/0957-4484/17/1/034

Yang C, Xu C, Wang X et al (2012) A displacement assay for the sensing of carbohydrate using zinc oxide biotracers. Electrochim Acta 60:50–54. doi:10.1016/j.electacta.2011.10.096

Zeng H, Cai W, Hu J et al (2006) Violet photoluminescence from shell layer of Zn/ZnO core–shell nanoparticles induced by laser ablation. Appl Phys Lett 88:171910. doi:10.1063/1.2196051

Zeng H, Duan G, Li Y et al (2010) Blue luminescence of ZnO nanoparticles based on non-equilibrium processes: defect origins and emission controls. Adv Funct Mater 20:561–572. doi:10.1002/adfm.200901884

Zhan X, Chen F, Salcic Z et al (2012) Synthesis of ZnO submicron spheres by a two-stage solution method. Appl Nanosci 2:63–70. doi:10.1007/s13204-011-0043-y

Zhang Z, Bian J, Sun J et al (2012) High optical quality ZnO films grown on graphite substrate for transferable optoelectronics devices by ultrasonic spray pyrolysis. Mater Res Bull 47:2685–2688. doi:10.1016/j.materresbull.2012.05.010

Zhang C, Zhou S, Li K et al (2013) Color-tunable ZnO quantum dots emitter: size effect study and a kinetic control of crystallization. Mater Focus 2:11–19. doi:10.1166/mat.2013.1042